Geomagnetic transport in the solar wind driven nightside magnetosphere–ionosphere system

W. Horton, C. Crabtree, I. Doxas, and R. S. Weigel

Citation: Physics of Plasmas (1994-present) **9**, 3712 (2002); doi: 10.1063/1.1499119
View online: http://dx.doi.org/10.1063/1.1499119
View Table of Contents: http://scitation.aip.org/content/aip/journal/pop/9/9?ver=pdfcov
Published by the AIP Publishing

Geomagnetic transport in the solar wind driven nightside magnetosphere–ionosphere system

W. Horton and C. Crabtree
Institute for Fusion Studies, The University of Texas at Austin, Austin, Texas 78712

I. Doxas
Department of Physics, University of Colorado, Boulder, Colorado 80309

R. S. Weigel
NASA/Goddard Space Flight Center, Greenbelt, Maryland 20771

(Received 4 April 2002; accepted 29 May 2002)

A spatially resolved nonlinear dynamical model of the solar wind driven geomagnetic tail plasma is developed for the purpose of space weather predictions. The model represents the fluctuating electromagnetic fields and high pressure central plasma sheet by a large number ($2N \lesssim 200$) of semiglobal coupled current loops ranging from the near-Earth geosynchronous orbit position for substorm dynamics to deep in the geotail. There is a spectrum of dynamical frequencies ranging from 1 h periods to 1 min and shorter periods. The low-frequency modes are global and lead to the dynamics of the low-dimensional ($d=6$) WINDMI model. The high-frequency dynamics are nonlinear compressional-rarefraction waves propagating up and down the geotail. The localized pulses start from sites of local reconnection set off either by the tearing mode unloading trigger or by localized solar wind disturbances acting on the nightside magnetopause. Larger unloading events lead to nonlinear steepening of the compressional pulsations which act to trigger secondary convection events under certain conditions. © *2002 American Institute of Physics.*
[DOI: 10.1063/1.1499119]

I. INTRODUCTION

A mathematical physics model that describes the multiscale coupling[1,2] in the flow of energy from the solar wind plasma through the magnetospheric plasma trapped by the Earth's geotail is presented and analyzed. For modes with the largest scales the dynamics of the system is shown to reduce to the low order space weather model called WINDMI,[3–5] which successfully describes the substorm global dynamics. The plasma electrodynamics is expressed in terms of many multiscale interacting current loops. The current loop topology is the natural mathematical expression for space weather input–output systems with feedback and feedforward pathways as already shown by the two loop WINDMI model. In WINDMI there is one large cross-tail current loop and one field-aligned current loop. In the present multiloop system there are new pathways from the largest scale to the smallest scale that are precisely expressed. While the local plasma is collisionless, and thus allows the sympletic Hamiltonian expressions for the particle dynamics, the essence of the space weather problem is a driven-dissipative system with bifurcations characteristic of such systems.

There is a broad societal and economic impact of having a reliable method of following the flow of charged particle energy from the sun through the Earth's magnetosphere to the ionosphere and the upper atmosphere. The input of power from the solar wind forms a large electrical dynamo in the geomagnetic tail delivering terawatts of power in quiet times to petawatts in disturbed times as the solar wind plasma velocity ranges from 300 to 800 km/s and varies in density and interplanetary magnetic field structure. Strongly disturbed magnetospheric conditions lead to economic losses from the failure of communication systems and electric utility distribution systems in northern latitudes. The multiscale model may provide a prediction capability that is more reliable for the less frequent, strong space weather events than earlier low-order models[6–8] and artificial intelligence network models.[9]

In Table I the global quantities that are discretized in the spatially resolved model presented here are reviewed with respect to their thermodynamic properties. All energy components, such as $p\Omega_{\rm cps}$, $\frac{1}{2}LI^2$, $\frac{1}{2}CV^2$ and $K_{\|}$, are extensive quantities. The reduction of the spatially resolved model to the $d=6$ global WINDMI occurs by the summation over the extensive quantities; $I=\Sigma_i^N\ I_i$, and the averaging over the intensive quantities

$$p=\frac{1}{N}\sum_i^N\ p_i$$

and

$$V=\frac{1}{N}\sum_i^N\ V_i\,.$$

This occurs when most of the energy settles into the largest scale modes of the system.

In Sec. II the spatially resolved dynamical model is described, the energy of the system is identified, and the energy conservation properties are described. In Sec. III the parallel computer code and numerical methods used to evaluate the

TABLE I. Thermodynamic properties of parameters and variables.

Extensive quantities	Intensive quantities
Ω_{cps} volume	p pressure
I current	V voltage
C capacitance	L inductance
$K_{\|}$ parallel flow energy	$u_{\|}$ parallel velocity
Σ conductance	σ conductivity

model is described and the first results of the onset of unloading events triggered by a constant solar wind driver are shown. The dynamics of compressional Alfvén pulses are then described and the energy transfer between the compressional magnetic disturbance and the plasma convection is described in some detail. In Sec. IV the eigenmode spectrum is analyzed and the prediction capability of the model is described. In Sec. V the conclusions are given.

II. SPATIALLY RESOLVED NONLINEAR DYNAMICS

The geotail is broken up into $2N$ cells known as simplexes in algebraic topology. Figure 1 shows the situation being described in the spatially resolved WINDMI model, each cell $\Delta x_i = x_i - x_{i-1}$ down the geotail contains dynamical equations for the current $I_i(t)$, cross-tail voltage $V_i(t)$, and the component of the normal $(\hat{z})$ magnetic field $B_i(t)$. The current I_i is equivalent to the contribution of the lobe magnetic field $B_{xi} = \mu_0 I_i(t)/\Delta x_i$. The total northward magnetic field is

$$B_z(x_i,t) = B_{\mathrm{dp}}(x_i) + B_i(x_i,t), \tag{1}$$

where B_{dp} is from the Earth's magnetic dipole.

There is a convection electric field given by $E_y(x_i,t) = V_i(t)/L_y$ where L_y could be taken as i-dependent, if required. Thus, there is an Earthward-directed Poynting flux of

$$S_i = \frac{1}{\mu_0} E_y(x_i,t) B_z(x_i,t) \tag{2}$$

in the model.

The current loops $I_i(t)$ now interact by the magnetic flux from the time-dependent magnetic dipole loop $A_i I_i$ at x_i through dipole loop $A_j I_j$ at x_j. This interaction is described by the geotail inductance matrix L_{ij} with

$$L_{ij} = \frac{\mu_0 A_i A_i}{[(x_i - x_j)^2 + R^2]^{3/2}} \tag{3}$$

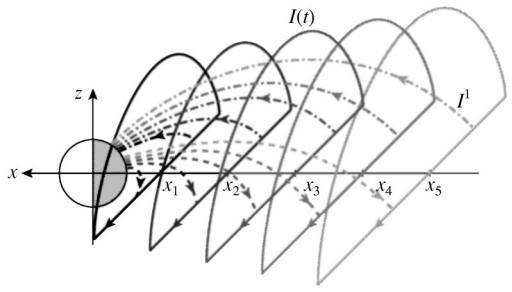

FIG. 1. Spatially resolved dynamical model with N cross-field and N field aligned current loops.

and the total lobe magnetic-energy in the geotail (gt) is given by

$$W_M^{\mathrm{gt}} = \frac{1}{2} \sum_{i,j}^{N} L_{ij} I_i I_j . \tag{4}$$

Thus W_M^{gt} is a discretized form of the magnetic field energy integral $\int_{\Omega_{\mathrm{gt}}} B^2 d^3x/2\mu_0$ taken over the geotail volume Ω_{gt}. It is straightforward to check that for $I_i = I/N = \text{constant}$ that Eq. (4) reduces to the original global model magnetic energy $W_M = \frac{1}{2}\mathcal{L} I^2$ with $\mathcal{L} = \mu_0 A/L_x$ where $A = A_i = \pi R^2/2$ and $L_x = N\Delta x$.

Allowing the solar wind driving voltage V_{sw}^i to depend on position x_i along the magnetopause we have the induction equation for the growth and decay of the currents in each cell

$$L_{ij} \frac{dI_j}{dt} = V_{\mathrm{sw}}^i - V^i + M_{ij} \frac{dI_j^1}{dt}, \tag{5}$$

where the matrix coupling $M_{ij} I_j^1$ replaces the single parallel $M-I$ coupling loop (M, I^1, V^1) of the global WINDMI model.[4]

Collecting all the components of the net dawn-to-dusk geotail cross-field currents gives the net current as the sum of the magnetohydrodynamic (MHD) current $\nabla p/B$, the polarization current $I_{pi}(t)$, and the off-diagonal momentum stress tensor $\nabla \cdot \pi/B$ driven current contribution. We get the finite-cell statement of the cross-field momentum balance equation. The details of the derivation follow those given in Ref. 3. The result is that perpendicular momentum balance in cell ω_i demands that

$$C_i \frac{dV_i}{dt} = I_i - I_i^1 - \frac{(B_i - B_{i-1})\Delta z}{\mu_0} - I_{pi}^{\mathrm{MHD}}(t) - \Sigma_i V_i . \tag{6}$$

This Eq. (6) is a statement of $F = ma$ for each current loop for the F perpendicular to **B**. From the point of view of circuits these momentum balance equations are statements of charge conservation with the algebraic sum of the currents into N-nodes equal to zero. The form of the two Kirchhoff equations is fundamental and intrinsically connected to the geometry of a system as is made clear in works on applied algebraic topology.[10,11] A more readable account of the simplexes and formulation of conservation laws by algebraic networks is given in Bamberg and Sternberg.[12]

Likewise the capacitance C of the central plasma sheet (CPS) is now the sum of the capacitances in cell ω_i of the CPS of volume $\Delta x_i L_y \Delta z_i$. The net polarization current in cell ω_i is

$$I_{pi}(t) = \int_{\omega_i} dx\, dz\, \frac{n_i m_i}{B^2} \frac{d}{dt}\left(\frac{V_i(t)}{L_y}\right), \tag{7}$$

where

$$B^2 = B_z^2(x_i,t) + (B'_{x_i} z)^2 . \tag{8}$$

Performing the integral with the approximation that $n_i \simeq n_i(x_i, z=0)$ over the range $\Delta z = B_z/B'_x = R_{ci}$ of the z integral, where R_{ci} is the radius of curvature of the magnetic field at $z=0$, we obtain from Eq. (7)

$$I_{pi}(t)=C_i\frac{dV_i}{dt} \tag{9}$$

with the cell plasma capacitance

$$C_i=\frac{\pi n_i(x_i)m_i\Delta x_i}{|B_z||B_x'|L_y}. \tag{10}$$

The global total polarization current is retrieved as $I_p=\Sigma_i I_{pi}=\Sigma_i C_i(dV/dt)$ when $V_i=V$ is independent of position along the tail. The total geotail capacitance C is given by $C=\Sigma_i C_i\sim 10^4$ F and the total inductance L is given by $L=\Sigma_{i,j}L_{ij}/N^2\sim 40$ H. The corresponding global oscillation period is $T_{\rm gt}=2\pi(LC)^{1/2}\sim 1$ h.

The spatially resolved dynamical model has oscillations of B_z about the mean $\langle B_z\rangle$ in both space and time. The growth in time of $B_z(x,t)$ occurs due to the difference $V_{i+1}-V_i$ and is given by Faraday's law applied to the B_z flux through $\Delta A_i=\Delta x_i L_y$. Thus, we get

$$\frac{\partial B_i}{\partial t}=-\frac{V_{i+1}-V_i}{\Delta x_i L_y} \tag{11}$$

and the change of the magnetic energy from B_z in cell ω_i is

$$\frac{\partial}{\partial t}\left[\frac{\omega_i B_{zi}^2}{2\mu_0}\right]=-\frac{(V_{i+1}-V_i)}{\mu_0}B_i(t)\Delta z. \tag{12}$$

The right-hand side of Eq. (12) is the Earthward divergence of the Poynting flux integral over the cell volume ω_i.

The dynamics of the spatially resolved dynamical system is given by

$$L_{ij}\frac{dI_j}{dt}=V_i^{\rm sw}-V_i(t)+M_{ij}\frac{dI_j^1}{dt}, \tag{13}$$

$$C_i\frac{dV_i}{dt}=I_i-I_i^1-\frac{(B_i-B_{i-1})\Delta z}{\mu_0}-I^{\rm MHD}(p_i)-\Sigma_i V_i, \tag{14}$$

$$\frac{\partial B_i}{\partial t}=-\frac{V_{i+1}-V_i}{\Delta x_i L_y}, \tag{15}$$

$$\frac{3}{2}\frac{dp_i}{dt}=\frac{\Sigma_i}{\Omega_i}V_i^2-u_{0i}\left(\frac{K_{\|i}}{\rho_i\Omega_i}\right)^{1/2}\Theta(I_i-I_{i,\rm cr})p_i, \tag{16}$$

$$\frac{dK_{\|i}}{dt}=I^{\rm MHD}(p_i)V_i-\frac{K_{\|i}}{\tau_\|}, \tag{17}$$

$$L_{ij}^1\frac{dI_j^1}{dt}=V_i-V_i^1+M_{ij}\frac{dI_j}{dt}, \tag{18}$$

$$C_i^1\frac{dV_i^1}{dt}=I_i^1-\Sigma_i^1 V_i^1. \tag{19}$$

There are six energy components of the dynamical model. The largest reservoir of energy is the total magnetic energy in the system which is given by the inductance matrices and current loops with I^1 field-aligned currents into the ionosphere and I cross-tail currents that are perpendicular to **B** in the geotail. The total system energy=magnetic+**E×B** flow+plasma+parallel flow energy. The magnetic energy equals the geotail energy plus the MI coupling energy. The **E×B** flow energy equals the geotail flows plus the MI coupling flows. There are seven distinct major energy components

$$E=\frac{1}{2}\sum_{i,j}\left[L_{ij}I_iI_j-M_{ij}I_iI_j^1+L_{ij}^1I_i^1I_j^1\right]+\sum_i\frac{B_i^2}{2\mu_0}\omega_i$$
$$+\frac{1}{2}\sum_i\left[C_iV_i^2+C_i^1(V_i^1)^2\right]+\sum_i\left(\frac{3}{2}p_i\Omega_i+K_{\|i}\right). \tag{20}$$

It is straightforward to show that the rate of change of the total energy in E associated with Eqs. (13)–(19) is determined by

$$\frac{dE}{dt}=I_i\cdot V_i^{\rm sw}-\Sigma_i^1(V_i^1)^2-u_{0i}\left(\frac{K_{\|i}}{\rho_i\Omega_i}\right)^{1/2}$$
$$\times\Theta(I_i-I_{i,\rm cr})p_i-\frac{K_\|}{\tau_\|}, \tag{21}$$

where there is a summation over the i index on the right-hand side. (Note that $\Sigma_i\Sigma_i^1$ are plasma conductances and not summation signs.) In the absence of solar wind driving and the loss terms, the energy transfer coupling elements cancel in pairs. In the conservative limit the system is Hamiltonian in structure.

III. COMPUTER SIMULATIONS OF COMPRESSIONAL ALFVÉN PULSES

A. Parallel numerical simulation

A parallel message passing code has been written for the Cray T3E at the Texas Advanced Computing Center to solve this new nonlinear dynamical model given by the system of Equations (13)–(19). Currently the $2N\times 2N$ inductance matrix is determined by the simple formula given by Eq. (3) and the $2N$ dimensional plasma capacitance vector (C_i,C_i^1) is given by Eq. (10). We use the Tsyganenko magnetic field model given in Ref. 13 to find partitions $\{x_i\}^N$ along the geotail that contain comparable amounts of current. For example, in Fig. 2 we show that the full $I\cong 20$ MA geotail current can be represented by $N=20$ cells carrying approximately 1 MA each. These partitions $\{x_i\}^N$ are then used to estimate the elements of the $2N\times 2N$ inductance matrix and the $2N$ dimensional plasma capacitance vector (C_i,C_i^1).

We follow a standard block cyclic distribution over the processor grid to utilize the PBLAS dense matrix software package to invert the block inductance matrix. We find that the partitioning of the geotail current $\{x_i\}^N$ must be chosen so that there is enough dispersion in the magnitude of the $L_{i,j}$ values that the condition number of the matrix does not exceed 10^3. Large condition numbers lead to numerical inaccuracies that cause the adaptive high order integrator to take increasingly smaller and smaller steps.

Figure 3 shows a series of stacked plots to indicate the evolution in time of the geotail voltage $V(x_i)$. In Fig. 3 the critical current is uniform independent of x_i as is the solar wind driving voltage. Avalanche-like behavior is seen to ini-

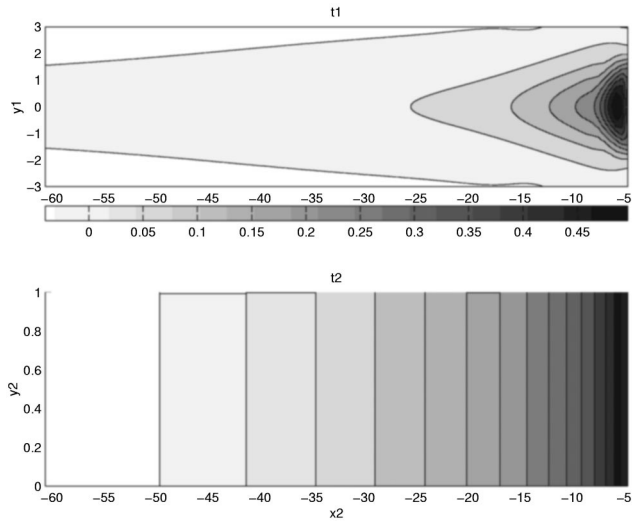

FIG. 2. A contour plot of the current density in units of MA/R_E^2 is shown in the top panel. Total current computed flowing through a region extending 1 R_E in the x direction, and 3 R_E above and below the equitorial plane in units of MA. All quantities are computed numerically from Tsyganenko's 1996 magnetic field model with the parameters, $ps=0.0$, $P_{\rm dyn}=3.0$, $D_{\rm st}=-150$, $B_y^{\rm IMF}=0.0$, and $B_z^{\rm IMF}=-10.0$.

tiate from five local reconnection sites. Other runs with a profile in $I_{i,\rm cr}$ show the avalanche starting at the lowest value of $I_{i,\rm cr}$.

B. Energy propagation through coupling

To understand the transport of energy from zone to zone by the compression-rarefraction pulse in detail, we need to write out two neighboring sets of energy equations. Consider that part of cross-field acceleration that arises from the north–south $B_i(t)$ field in cells ω_i and ω_{i+1}, let us form four subenergy components from Eqs. (20) and (21):

$$\frac{d}{dt}\left(\frac{1}{2}C_iV_i^2\right)=\frac{\Delta x_iB_{x_i}V_i}{\mu_0}-V_i(B_i-B_{i-1})\Delta z/\mu_0, \tag{22}$$

$$\frac{d}{dt}\left(\frac{1}{2}C_{i+1}V_{i+1}^2\right)=\frac{\Delta x_{i+1}B_{x_{i+1}}V_{i+1}}{\mu_0}-V_{i+1}(B_{i+1}-B_i)\Delta z/\mu_0, \tag{23}$$

$$\frac{d}{dt}\left(\frac{\Delta xL_y\Delta zB_i^2}{2\mu_0}\right)=-B_i(V_{i+1}-V_i)(\Delta z/\mu_0), \tag{24}$$

$$\frac{d}{dt}\left(\frac{\Delta xL_y\Delta zB_{i+1}^2}{2\mu_0}\right)=-B_{i+1}(V_{i+2}-V_{i+1})(\Delta z/\mu_0). \tag{25}$$

Now focus on the coupling through the V_iB_j terms and ignore the input in each cell from the B_xV due to the north–south Poynting flux. From Eq. (22) we see that the input energy is $V_iB_{i-1}\Delta z/\mu_0$, the coupling power from $\frac{1}{2}C_iV_i^2$ to $\omega_iB_i^2/2\mu_0$ is $V_iB_i\Delta z/\mu_0$, and the output energy is $B_iV_{i+1}\Delta z/\mu_0$ in the cell ω_i. The output of cell ω_i is then the input power in Eq. (24) to convection in cell ω_{i+1}. Now the coupling events described for ω_i are repeated for cell ω_{i+1}.

Forming the rate of change of the total of the **E×B** convection and compressional magnetic energy in cells ω_i and ω_{i+1} from Eqs. (22) through (24), and dropping the standard WINDMI power input terms from $I_iV_i=\Delta x_iB_{xi}V_i/\mu_0$ for clarity, we get from the energy components

$$\frac{d}{dt}\left(\frac{1}{2}C_iV_i^2+\frac{\omega_iB_i^2}{2\mu_0}\right)=\frac{V_iB_{i-1}\Delta z}{\mu_0}-\frac{B_iV_{i+1}\Delta z}{\mu_0}, \tag{26}$$

$$\frac{d}{dt}\left(\frac{1}{2}C_{i+1}V_{i+1}^2+\frac{\omega_{i+1}B_{i+1}^2}{2\mu_0}\right)=\frac{V_{i+1}B_i\Delta z}{\mu_0}-\frac{B_{i+1}V_{i+2}\Delta z}{\mu_0}. \tag{27}$$

Thus, the terms $B_iV_{i+1}\Delta z/\mu_0$ transfer power out of cell ω_i into cell ω_{i+1}. So the total two-cell geotail energy conservation law is now

$$\frac{d}{dt}(W_i+W_{i+1})=\sum_{i=1,2}\frac{\Delta x_iB_{x_i}V_i}{\mu_0}+\frac{V_iB_{i-1}\Delta z}{\mu_0}-\frac{V_{i+2}B_{i+1}\Delta z}{\mu_0}. \tag{28}$$

For N cells, the terms are the same as those identified previously, but the input flux is pushed off to the deep tail where the first input term $V_1B_0\Delta z/\mu_0$ is small and the last outflow term is at the near-Earth boundary of the central plasma sheet. The outflow and power to the nightside region 1 current can be large due to the input of energy along the length of the geotail. When the unloading trigger is set off a large burst of power is released and it propagates nonlinearly along both directions in the geotail plasma. A more elaborate treatment of the near-Earth boundary would include the Alfvén layer separatrix crossing physics. This physics should be expanded to include the generation of additional I_i^1 currents from the dawn–dusk pressure gradient as described by Ref. 14. A more accurate interfacing surface between the roughly axisymmetric dipolar region and the geotail plasma is a high priority for the next level of description.

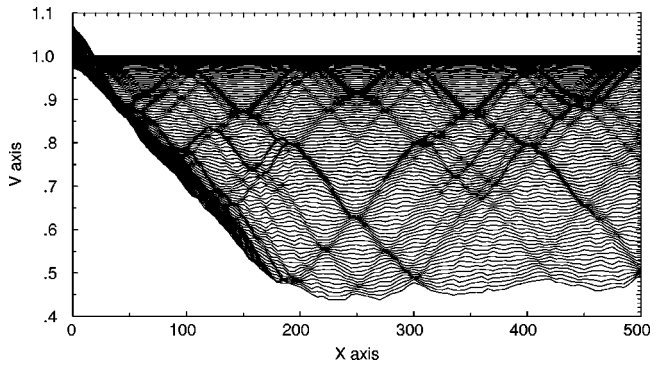

FIG. 3. Time evolution of the cross-tail convection voltage for $\delta x=5R_e$ and $N=100$ with a constant solarwind driving voltage and a constant critical current. There are five positions at which the unloading starts resulting in a complex pattern of Earthward and tailward pulses.

IV. PREDICTION OF GEOTAIL CURRENTS-VOLTAGES FROM THE MODEL

Here we estimate the expected spectrum of oscillations and the currents and voltages given by the model for typical magnetospheric parameters.

A. The eigenmodes of geotail system

Consider the reduced equation

$$L_{ij}\frac{d^2I_j}{dt^2}=\dot{\mathcal{E}}_i^{\rm sw}-\frac{1}{C_i}[I_i-I_p(i)-\Sigma_i V_i],$$
$$L_{ij}\ddot{I}_j+\frac{1}{C_i}I_i=\dot{\mathcal{E}}_i^{\rm sw}+\frac{I_p(i)}{C_i}. \tag{29}$$

The right-hand side may be for example 10^4 V/10^3 s $+10^5$ A/10^4 F giving 20 V/s with comparable contributions.

Solutions are sought in the form of oscillations along the tail

$$I_j=I_0(t)e^{ik_xx_j}+\text{c.c.}$$

for in the approximation that $L_{ij}=L(i-j)$ since $\Sigma L_{ij}e^{ik_x(x_j-x_i+x_i)}=e^{ik_xx_i}L(k_x)$. We obtain the homogeneous equations for $I_0(t)$,

$$\ddot{I}_0+\frac{1}{CL(k_x)}I_0=0, \tag{30}$$

for the limit $C_i=C$. Then the spectrum of oscillations is

$$\omega^2(k_x)=\frac{1}{CL(k_x)}=\frac{1}{C\mu_0\pi R[k_xRK_1(k_xR)]}. \tag{31}$$

In Eq. (31) we use

$$\int_0^\infty\frac{\cos(ax)dx}{(\beta^2+x^2)^{3/2}}=\frac{a}{\beta}K_1(a\beta)$$

and

$$L(k_x)=2\int_0^\infty\frac{dx}{L_x}\frac{\mu_0A^2\cos(k_xx)}{(x^2+R^2)^{3/2}}$$
$$=\frac{2\mu_0A^2}{L_x}\left[\frac{k_xK_1(k_xR)}{R}\right]$$
$$=\frac{2\mu_0A\pi}{L_x}[k_xRK_1(k_xR)]\to\frac{2\pi\mu_0A}{L_x},\quad k_xR\to0. \tag{32}$$

Thus, there is an N-dimensional spectrum of geotail eigenmodes and eigenvectors for N cells.

B. Nonlinear compressional signals along the geotail

The higher-order modes in the N-degree of freedom spatially resolved dynamical model describe the propagation Earthward and the reflection from the dipolar region of nonlinear compressional Alfvén signals. We avoid the use of the word ''wave'' here since the subhertz dynamics of the disturbances is better described by localized traveling pulses. The most important nonlinearity for these signals arises from Eqs. (1) and (9) where we see that compressional regions with $\delta B_i\propto\delta p_i>0$ have a lower polarization current and plasma capacitance. This nonlinearity in the capacitance leads to the steepening of the front of the Earthward propagating pulses. For an initial pulse of width $\Delta x\ll|x_N-x_0|=L_x$ and amplitude $\delta B_i(t=0)$ at position x_i, the forward edge steepens due to the nonlinearity of $C(B_z)$ which gives locally the amplitude modulated signal speed $\omega/k_x=v_{\rm A}(1+(\delta B/B_z))$. Thus, the front edge of the pulse, when arriving at the (NGO) transition region x_N between the geotail and the inner magnetosphere can have a much smaller width $\Delta x(L_N)=\Delta x(L_N)=\Delta x-\delta v_{\rm A}t=\Delta x-|x_N-x_0|(\delta B/B)$ for a finite initial amplitude disturbance set off by the trigger in a geotail dipole loop at x_0 or from some direct solar wind-induced voltage pulse at x_0. Here, we used the expression $\delta v_{\rm A}=v_{\rm A}\delta B/B$ where the Alfvén velocity in each cell $v_{\rm A}$ is controlled by $1/[\mu_0C(B_z)]^{1/2}$. The variation of the Alfvén speed over the pulse width Δx and the propagation time $t_N=|x_N-x_0|/v_{\rm A}$ for the pulse to reach x_N from x_0. Clearly, to follow in detail the steepening of the pulse front requires smaller and smaller cells. In the limit of $\Delta x_i\to0$ the description parallels that of the Burger equation.[15] A formal description of this one aspect of the problem (the steepening fronts) can be given by the Burger equation with suitable initial data. In the geotail the collisionless viscosity term for the Burger equation model is very low so that the calculation of the steepening in the differential equation limit is that given by Whitham in the high Rayleigh number regime.

What is not simple in the geotail model is the coupling of the pulse through the multipole WINDMI model energy components to the ionosphere. There are many other degrees of freedom and particularly difficult is the transmission and reflection of the pulses by the ionosphere. Thus the computer solutions of the system of linked dynamical equations are useful.

From the simulations we see the expected steepening of the Earth propagation pulses $E_y^{(1)}(x-v_{\rm A}t)$ and $\delta B_z^{(1)}(x-v_{\rm A}t)$ with the energy density $W_i=\omega_i\delta B_i^2/2\mu_0+\frac{1}{2}CV_i^2(t)$ and the energy flux given in Eq. (2). In the reflected signal, the magnetic pulse $\delta B_z(x+v_{\rm A}t)$ changes sign while the electric pulse $\delta E_y(x+v_{\rm A}t)$ remains positive (dawn-to-dusk). What fraction of energy is transmitted to the region 1 current loops and the inner magnetosphere appears highly variable.

The steepened front edge of the Earthward propagation compressional pulse both steepens the Earthward pressure gradient $p(x-x_N,t)$ and then produces an abrupt increase in the B_z. The steepened pressure gradient would appear to be sufficient to push the Tsyganenko pressure gradients calculated in Refs. 16–18 into the unstable interchange motion. In this scenario the reconnection at $x=-15\pm5\,R_e$ occurs first and the kinetic ballooning second as a consequence of the steepened gradient. The inverse order of events is also allowed in the model if the trigger condition for unstable interchange is set off before the near-Earth neutral-line trigger in the geotail. This is the order of the events argued for in Ref. 19 based on the Combined Release and Radiation Effects Satellite (CRRES) data. The tailward propagating rarefaction pulse with $\delta B_i<0$ will then trigger the reconnection event when the conditions in the geotail are favorable. In other unfavorable conditions the plasmoid would not form

consistently with other observations. We need more experience with the new model to decide which set of conditions can better model certain correlated datasets.

C. Cross-tail current for geotail cell $X_{i+1}-X_i$

For the main component of the cross-tail current we estimate that

$$I_i = C_i\frac{dV}{dt} + I_p(i) + \Sigma_i V_i = \underbrace{2\times 10^3 F\cdot \frac{5\times 10^4 V}{50\ s}}_{2\mathrm{MA}} + V\Delta p + 3\ \mathrm{mho}\cdot 5\times 10^4\ \mathrm{V} \tag{33}$$

where

$$V = \int \frac{ds}{B} = 3\times 10^{16}\ \mathrm{m^2/Wb}$$

is the flux tube volume. For $\Delta p > 1$ nPa we get $V\Delta p$ is 30 MA. Consider the power transfer from the currents $I_p(i)$ and $\Sigma_i V_i$ to the thermal pressure and the parallel flows.

From the ordinary differential equations this is

$$C_i\frac{dV_i}{dt} = I_i - I_p(i) - \Sigma_i V_i,$$
$$\frac{3}{2}\Omega_i\frac{dp_i}{dt} = \Sigma_i V_i^2 - \frac{p_i\Omega}{\tau_E}, \tag{34}$$

yielding

$$\frac{d}{dt}\int_{\omega_i}\left(\frac{1}{2}\rho V_E^2 + \frac{3}{2}p\right)d^3x = \frac{d}{dt}\left[\underbrace{\frac{1}{2}C_i V_i^2 + \frac{3}{2}\Omega_i p_i}\right]$$
$$= \underbrace{V_i I_i}_{\text{input power}\sim 10^{12}\ \mathrm{W}} - V_i I^{\mathrm{MHD}}(p_i) - \frac{p_i\Omega_i}{\tau_E} \tag{35}$$

where $V_i I^{\mathrm{MHD}}(p_i)$ is the transfer to $K_\parallel$ unloading power, $\Sigma_i V_i^2$ is the energy transfer from **E×B** flow kinetic energy to thermal pressure energy through the collisionless viscosity.

Now, the power $V_i I^{\mathrm{MHD}}(p_i)$ drives up $K_{\parallel i} = \frac{1}{2}\int \rho_i u_{\parallel i}^2 d^3x$ parallel kinetic energy at x_i.

D. Estimates of the voltages during sudden events

Consider the following system parameters:

$$R = \frac{H}{2} \cong 10R_E \sim 6\times 10^7\ \mathrm{m},$$
$$x_{ij} = 10R_E, \tag{36}$$
$$L_{ij} = 2\times 10^{-7}\frac{\pi^2 R_E^4}{2^{7/2}R_E^3} \cong 40\ \ \mathrm{H}.$$

This is a rough estimate (upper bound) to the values of L_{ij}. We show in Fig. 2 the values obtained from Tsyganenko 96 using 20 bins of 1 MA per bin for a particular D_{st} and given value of interplanetary magnetic field (IMF) parameters. Earlier studies gave $L_{ij} \to 30$ H. We note from Table I that L is an intensive quantity so that the global value is the average of the local value.

Now during the growth phase the current ramp-up is bounded by $\dot{I} = 1\ \mathrm{MA}/100\ \mathrm{s} = 10^4$ A/s then $\mathcal{E} = L\dot{I} = 30H \times 10^4$ A/s $= 3\times 10^5$ V, which is a large transient voltage. During the voltage pulse the flux tubes move inward according to

$$\psi = B_n x - B_x' z^2/2 - \mathcal{E}t \tag{37}$$

and the pressure and current grow as

$$j_{1+1/2} = \frac{1}{B_n}\frac{dp}{dx} = \frac{p_{i+1}-p_i}{B_n(x_{i+1}-x_i)} = \frac{\partial p_{(i+1/2)}}{\partial\psi} \tag{38}$$

and

$$I(p_i) = \int_{\omega_i} dr_\perp ds j = \int \frac{ds}{B}\left[d\Psi\frac{\partial p}{\partial\Psi}\right] = \Delta p V(\Psi). \tag{39}$$

E. Cross-tail current contributions from the collisionless off-diagonal momentum stress tensor

We know that the current density is given by

$$j = j_{\mathrm{pol}} + \frac{1}{B_n}\frac{\partial p}{\partial x} + \sigma E_y, \tag{40}$$

where $j_{\mathrm{pol}} = (\rho_m/B)d/dt(E_y/B)$. The cross-tail current sources give using $E_y = V(t)/L_y$,

$$I = \int da\, j = \int \frac{dx\, dz\, \rho m}{B^2}\frac{d}{dt}\left(\frac{V}{L_y}\right) + \int dx\, dz\frac{1}{B_n}\frac{\partial p}{\partial x} + \Sigma V. \tag{41}$$

Now the electrical conductance Σ of the central plasma sheet (CPS) is the integrated, nonlocal

$$\Sigma V = \underbrace{\int dxdz\sigma\frac{V}{L_y}}_{\Sigma\ \text{conductance} = \frac{A_{\text{area}}\,\sigma}{L_y}} \cong L_y^{-1}\left(\int dxdz\sigma\right)V(t) \tag{42}$$

where σ is the effective conductivity of the CPS[4] from the divergence of the off-diagonal momentum stress tensor. Thus, we use the formula

$$\Sigma = 0.1\left[\frac{n_e e}{B_n}\right]\left(\frac{\rho_i}{L_z}\right)^{1/2}(\mathrm{mho/m}) \tag{43}$$

from the calculations in Ref. 5. Typical CPS values then give

$$\Sigma = \frac{\Delta x\Delta z}{L_y}\sigma \sim 30\ \ \mathrm{mhos}.$$

Thus for $V = 10$ kV we get $\Sigma V = 0.3$ MA and for $V = 100$ kV, $\Sigma V = 3$ MA and $\Sigma V^2 = 3\times 10^{11}$ W. This current, while small, compare to the MHD current

$$I^{\mathrm{MHD}}=\int dx\,dz\,\frac{1}{B_n}\frac{\partial p}{dx}$$
$$=\int \frac{ds\,dr_\perp B}{B}\frac{\partial p}{\partial \psi}$$
$$=\int d\psi V\frac{\partial p}{\partial \psi}=\sum_i \Delta p_i V_i \simeq 10 \ \mathrm{MA} \tag{44}$$

is the one that drives the irreversible heating of the plasma. The ion-inertial polarization current energizes the cross-field convection $\rho_m v_E^2/2$,

$$I_{\mathrm{pol}}=\int \frac{dx\,dz\,\rho_m(z)}{L_y(B_n^2+B_x'^2 z^2)}\frac{dV}{dt}$$
$$=\frac{\pi\Delta x}{L_y}\frac{\rho_m(0)}{B_n B_x'}\frac{dV}{dt}\cong C\frac{dV}{dt}\leqslant 1 \ \mathrm{MA}. \tag{45}$$

F. Calculation of the plasma capacitance distributed along the geotail

Consider the mass density ρ_m from protons in the central plasma sheet

$$C: \quad \rho_m=1.67\times10^{-27}\ \mathrm{kg}\times10^{6}\ \mathrm{m}^{-3}$$
$$=1.67\times10^{-21}\ \mathrm{kg/m}^3.$$

The CPS capacitance is determined by ρ_m and the field components

$$B_z=10^{-9}\ \mathrm{T}, \quad B_x'/\mu_0=\frac{20\times10^{-9}}{2R_E\times10^{-6}}=1.6\ \mathrm{nA/m}^2.$$

Thus, we estimate that

$$C_i=\frac{3.14(1.67\times10^{-21}\ \mathrm{kg/m}^3)3\times10^{7}\ \mathrm{m}}{6\times10^{7}\ \mathrm{m}(10^{-9}\mathrm{T})\frac{1}{6}10^{-14}\ \mathrm{T/m}}$$
$$=16.7\times10^{-21-9+14}=1670\ \mathrm{F}\sim 2000\ \mathrm{F}.$$

For the total C we get for the $C=\Sigma_i C_i=10^4$ F or more.

G. Earthward gradients of the particle distribution functions with solar wind variation

In this section we compute the Earthward gradient of the pressure distribution function $p(x_i,t)$ for a varying E_y representing a half cycle pulse of E_y in the distant neutral-line (DNL) region.

The distant neutral line DNL is a source region for entry of new solar wind ions into the geotail which we model as $S_{\mathrm{DNL}}(x,t)=S_{\mathrm{DNL}}(t)\,\delta(x-x_{\mathrm{DNL}})$. Near the geosynchronous orbits there is a sink of ions with respect to the geotail plasma. The ions cross from the geotail region into the inner magnetosphere through the Alfvén layer seperatrix. The ions are also lost through the dusk side low latitude boundary layer. We write this net loss region as $S_{\mathrm{NE}}(t)\,\delta(x-x_{\mathrm{NE}})$ for the near Earth (NE) loss region.

Now the transport of ions is through the Earthward convective flow $u_x=E_y/B_z(x)$ and a turbulent velocity space diffusive flux is $-D_\Psi\partial p/\partial\Psi$. Thus, the one-dimensional model for the pressure distribution function is

$$\frac{\partial p}{\partial t}=-\frac{\partial}{\partial\Psi}\left(E_y p-D_\Psi\frac{\partial p}{\partial\Psi}\right)+S_{\mathrm{DNL}}(t)\,\delta(x-x_{\mathrm{DNL}})$$
$$-S_{\mathrm{NE}}(t)\,\delta(x-x_{\mathrm{NE}}), \tag{46}$$

where D_Ψ is the turbulent diffusivity due to low frequency drift wave turbulence. We estimate the value of D_Ψ through

$$D_\Psi=\frac{\langle\delta\Psi^2\rangle}{\tau_C}=B_z^2\frac{\langle\delta x^2\rangle}{\tau_C}, \tag{47}$$

where $\langle\delta x^2\rangle$ is the dominate wavelength in the fluctuation spectrum and τ_C is the correlation time. The associated local **E×B** turbulent diffusivity is

$$D_x=\langle\delta x^2\rangle^{1/2}\langle\tilde v_E^2\rangle^{1/2}=\frac{\langle\delta x^2\rangle}{\tau_C}. \tag{48}$$

For $\langle\delta x^2\rangle\propto\rho_i L_p\approx(300\ \mathrm{km})(10^4\ \mathrm{km})=3\times10^6\ \mathrm{km}^2$ and $\tau_C\approx100$ s we estimate that $D_x=3\times10^4\ \mathrm{km}^2/\mathrm{s}$. This compares with Borovsky's MHD estimate of $D_\perp\approx10^7\ \mathrm{km}^2/\mathrm{s}$. The corresponding $D_\Psi=0.3(\mathrm{nT}R_e)^2/\mathrm{s}$, taking $B_z=20$ nT gives a solution of Eq. (46),

$$\frac{1}{p}\frac{\partial p}{\partial\Psi}=\frac{E_y}{D_\Psi}=\frac{1\,\frac{\mathrm{mV}}{m}}{0.3(\mathrm{nT}R_e)^2/\mathrm{s}}=0.5\frac{1}{\mathrm{nT}R_e}. \tag{49}$$

Thus, we estimate the characteristic drift wave frequency as

$$\omega_*=-k_y\frac{\langle E\rangle}{qp}\frac{\partial p}{\partial\Psi}\leqslant k_y\rho_i\frac{v_i}{L_f}. \tag{50}$$

For $L_p^{-1}=\partial_x\log p$ from Eq. (49) used in Eq. (50) we get,

$$\omega_*=k_y\rho_i\frac{400\ \mathrm{km/s}}{10^4\ \mathrm{km}}=0.04k_y\rho_i\ \mathrm{rad/s},$$

$$f_*=k_y\rho_i 6\ \mathrm{mHz}.$$

Typically, the fastest growing waves have $k_y\rho_i\approx0.4$–1.0. Figure 4 shows a steepening of the pressure gradient as a pressure front propagates toward the Earth from a disturbance in the distant geotail. The pressure pulse drifts Earthward rapidly until it reaches the dipole breaking region where it slows down and the pressure piles up. Steep gradients near the geosynchronous orbit are thought to trigger flux-tube convection and auroral brightening.[16,20–24]

V. CONCLUSIONS

A spatially resolved nonlinear dynamical model of the solar wind driven geomagnetic tail plasma is developed for the purpose of space weather predictions. Through a finite, but potentially large number of coupled ordinary differential equations, the model describes the solar wind driven magnetosphere–ionosphere system through the plasma-electrodynamics. The model builds on the six-dimensional WINDMI model by breaking up the large currents in that semi-global model into a large number of spatially resolved

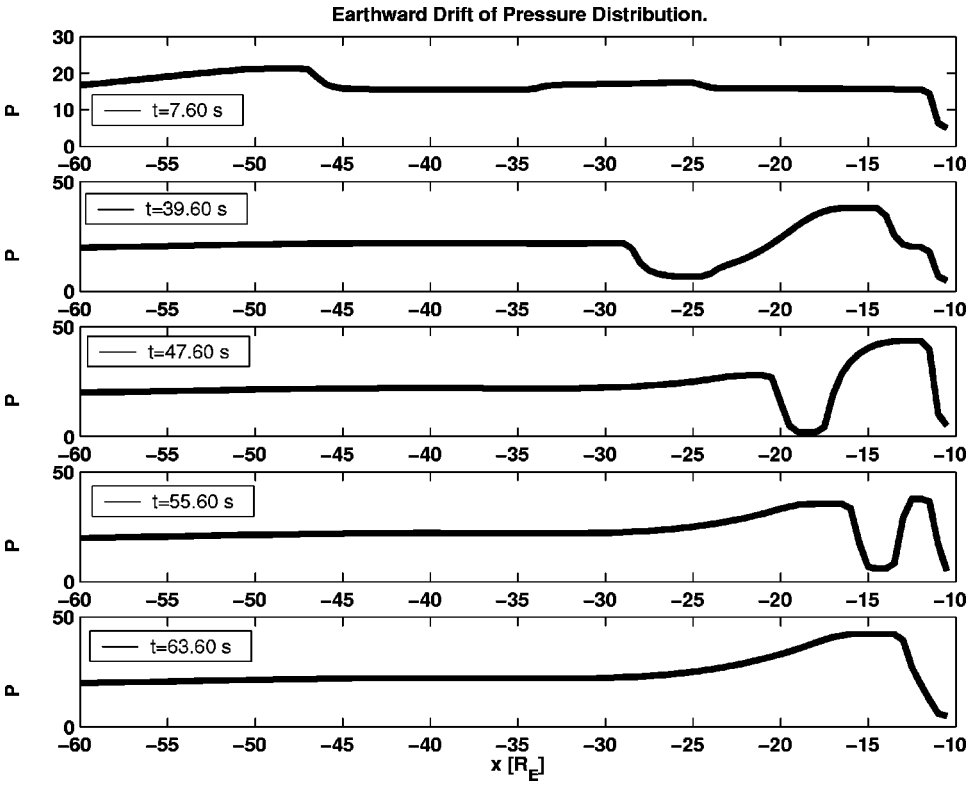

FIG. 4. Earthward transport of pressure, with tailward source oscillating through one full period of a cosine wave. Due to the Earthward decrease in the $\mathbf{E}\times\mathbf{B}/B^2$ velocity, from the increasing $B_z(x)$ the pressure piles up in the tail/dipole transition region. The top panel shows the pressure profile for a time very soon after the initial conditions, where the pulse is traveling Earthward (to the right). The bottom panels show later times as the pulse reaches the dipole region and the pressure gradients become large.

current loops. Thus, the new model has ($2N \lesssim 200$) eigenfrequencies for the linearized system that range in time scales from minutes to hours. The higher frequency 1 min oscillations would couple to the drift wave oscillations being pursued in a related work. These small-scale fast oscillations become nonlinear at low amplitudes and are part of the compressional pulses described in Sec. IV A. The low-frequency modes are global in nature and lead to the dynamics similar to that of the low-dimensional ($d=6$) WINDMI model. An example of the way the WINDMI model can reproduce a substorm event is shown in Fig. 5.

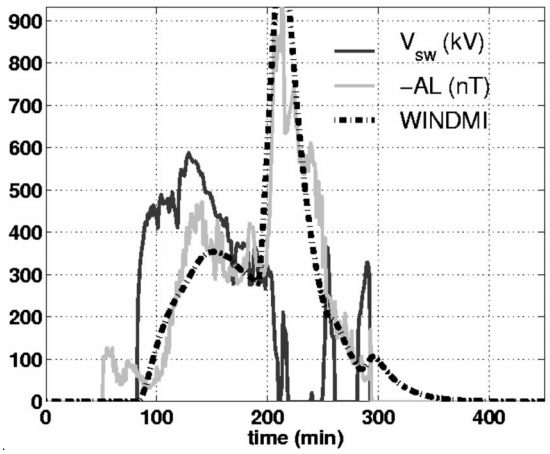

FIG. 5. The optimized global WINDMI system with two current loops in a $d=6$ state space captures the rapid rise in *AL* that begins at $t=200$ min. The *ARV* is 0.12. Substorm example from the Blanchard–McPherron dataset (18 August 1978).

The localized pulses start from sites of local reconnection set off by the tearing mode unloading trigger as shown in Fig. 3. Large energy unloading events can apparently be set off either by localized solar wind disturbances acting on a loaded magnetosphere or through the load stressing the geotail reversed field to the point where the internal reconnection trigger is fired. The later case for a constant solar wind driver is shown in Fig. 3.

High energy unloading events lead to nonlinear steepening of the compressional pulsations which tend to act to trigger secondary events under certain conditions.

Due to the nonlinear steepening it is likely that the system shows self-organized criticality: however this is not certain and will require that a library of computer runs with good space–time diagnostics be assembled to determine what is the characteristic frequency spectra in the strongly driven system and what are the bifurcation patterns. Only recently have the bifurcation patterns and fractal character of the boundary between limit cycles and chaotic zones been determined for the low order WINDMI model.[25,6]

The question arises as to how a more systematic formulation of the conservation laws can be formulated for general decompositions of the geotail system. Bamberg and Sternberg[12] use this fact to introduce algebraic topology through the systematic fomulation of complex networks in their text book on mathematical physics. Electrical networks are of more general mathematical-physics importance than might be first recognized. Kirchoff's two laws: that (i) the algebraic sum of the currents at each node is zero and (ii) the algebraic sum of the voltages around a loop is zero follow from the first theorems of algebraic topology.[10]

ACKNOWLEDGMENTS

This work was supported by National Science Foundation Grant No. ATM-9907637 and U.S. Department of Energy Contract No. DE-FG03-96ER-54346.

[1]S.-I. Akasofu, Planet. Space Sci. **28**, 295 (1980).
[2]D. N. Baker, T. I. Pulkkinen, J. Büchner, and A. J. Klimas, J. Geophys. Res., [Space Phys.] **104**, 14601 (1999).
[3]W. Horton and I. Doxas, J. Geophys. Res., [Space Phys.] **101**, 27223 (1996).
[4]W. Horton and I. Doxas, J. Geophys. Res., [Space Phys.] **103**, 4561 (1998).
[5]W. Horton, M. Pekker, and I. Doxas, Geophys. Res. Lett. **25**, 4083 (1998).
[6]R. S. Weigel, Ph.D. thesis, The University of Texas at Austin, 2000.
[7]D. Vassiliadis, A. J. Klimas, D. N. Baker, and D. A. Roberts, J. Geophys. Res., [Space Phys.] **100**, 3495 (1995).
[8]D. R. Weimer, J. Geophys. Res., [Space Phys.] **99**, 11005 (1994).
[9]R. S. Weigel, W. Horton, T. Tajima, and T. Detman, Geophys. Res. Lett. **26**, 1353 (1999).
[10]Lefschetz and Solomon, *Applications of Algebraic Topology* (Springer, New York, 1975), p. 189.
[11]Lefschetz and Solomon, *Applications of Algebraic Topology: Graphs and Networks: The Picard-Lefschetz Theory and Feynman Integrals* (Springer, New York, 1975), pp. 1884–1972.
[12]P. Bamberg and S. Sternberg, *A Course in Mathematics for Students of Physics* (Cambridge University Press, Cambridge, MA, 1990), pp. 407–474.
[13]N. A. Tsyganenko and D. P. Stern, J. Geophys. Res., [Space Phys.] **101**, 27187 (1996).
[14]L. R. Lyons, J. Geophys. Res., [Space Phys.] **100**, 19069 (1995).
[15]G. B. Whitham, *Linear and Nonlinear Waves* (New York, Wiley, 1974).
[16]W. Horton, H. V. Wong, J. W. Van Dam, and C. Crabtree, J. Geophys. Res., [Space Phys.] **106**, 18803 (2001).
[17]W. Horton, J. P. Smith, R. Weigel, C. Crabtree, I. Doxas, B. Goode, and J. Cary, Phys. Plasmas **6**, 1 (1999).
[18]W. Horton, H. V. Wong, and J. W. Van Dam, J. Geophys. Res., [Space Phys.] **104**, 22745 (1999).
[19]G. M. Erickson, N. C. Maynard, W. J. Burke, G. R. Wilson, and M. A. Heinemann, J. Geophys. Res., [Space Phys.] **105**, 25265 (2000).
[20]L. A. Frank and J. B. Sigwarth, J. Geophys. Res., [Space Phys.] **105**, 12747 (2000).
[21]L. A. Frank, W. R. Paterson, J. B. Sigwarth, and S. Kokubun, J. Geophys. Res., [Space Phys.] **105**, 15897 (2000).
[22]L. A. Frank, J. B. Sigwarth, and W. R. Paterson, in *Substorms-4*, edited by S. Kokubun and Y. Kamide (Kluwer Academic, Norwell, MA, 1998), pp. 3–8.
[23]A. T. Y. Lui and J. S. Murphree, Geophys. Res. Lett. **25**, 1269 (1998).
[24]P. L. Pritchett and F. V. Coroniti, J. Geophys. Res., [Space Phys.] **104**, 12289 (1999).
[25]J. P. Smith, J.-L. Thiffeault, and W. Horton, J. Geophys. Res., [Space Phys.] **105**, 12983 (2000).